Inorg. Chem. **2000,** *39,* 5354−5364

Structural Origin of Two Paramagnetic Species in Six-Coordinated Nitrosoiron(II) Porphyrins Revealed by Density Functional Theory Analysis of the g Tensors

S. Patchkovskii and T. Ziegler*

Department of Chemistry, University of Calgary, 2500 University Dr. NW,
Calgary, Alberta, T2N 1N4 Canada

Received May 26, 2000

Potential energy and electron paramagnetic resonance (EPR) **g** tensor surfaces of model five- and six-coordinated porphyrins were examined. For both types of complexes, the NO ligand is preferably coordinated end-on, with a Fe−N−O bond angle of approximately 140°. In the free five-coordinated structure, NO undergoes free rotation around the axial Fe−N(NO) bond. This motion is strongly coupled to the saddle-type distortion of the porphyrin ligand. Coordination by the second axial ligand (imidazole) raises the calculated barrier for NO rotation to about 1 kcal/mol, which is further increased by displacements of imidazole from the ideal axial position. The potential energy surface for the dissociation of the weakly coordinated imidazole ligand is exceptionally flat, with variation of the Fe−N(Im) bond length between 2.1 and 2.5 Å changing the energy by less than 1 kcal/mol. Experimental orientations of both axial ligands, as well as the Fe−N(Im) bond length, are therefore likely to be determined by the environment of the complex. In contrast to the total energy, calculated EPR **g**-tensors are sensitive to the orientation of the NO ligand and to the Fe−N(Im) bond length. Contrary to a common assumption, the **g** tensor component closest to the free-electron value does not coincide with the direction of the Fe−N(NO) bond. From comparison of the calculated and experimental **g**-tensor components for a range of structures, the rhombic ("type I") EPR signal is assigned to a static structure with NO oriented toward the meso-C atom of the porphyrin ring, and $R_{\mathrm{Fe-N(Im)}} \approx 2.1$ Å (calcd $g_1 = 1.95$, $g_2 = 2.00$, $g_3 = 2.04$; exptl $g_1 = 1.96-1.98$, $g_2 = 2.00$, $g_3 = 2.06-2.08$). The axial ("type II") EPR signal cannot correspond to any of the static structures studied presently. It is tentatively assigned to a partially dissociated six-coordinated complex ($R_{\mathrm{Fe-N(Im)}} > 2.5$ Å), with a freely rotating NO ligand (calcd $g_{\|} = 2.00$, $g_{\perp} = 2.03$; exptl $g_{\|} = 1.99-2.00$, $g_{\perp} = 2.02-2.03$).

I. Introduction

Iron-containing porphyrin complexes (hemes) serve as prosthetic groups in many vitally important enzymes.[1,2] Two of the heme-based oxygen transport enzymes, hemoglobin and myoglobin, are arguably among the most intensively studied biological molecules.[3] Because oxyhemoglobin possesses a singlet electronic structure, it is not amenable to studies using electron paramagnetic resonance (EPR) and electron−nuclear double resonance (ENDOR).[4] However, structurally similar heme nitrosyls have a spatially nondegenerate spin-doublet ground state, which is readily observable with EPR, and provide a useful model for oxyheme species.[5] Moreover, nitrosoiron porphyrins serve several important biological functions in their own right.[6−8] As a consequence, both structures and magnetic resonance properties of nitroso complexes of heme-containing enzymes, and several model complexes, have been extensively studied over the past 30 years. These complexes continue to attract considerable experimental attention.[9−22]

Experimental EPR spectra of nitrosylated hemoglobins and myoglobins,[4,5,14,23−26] as well as of some model complexes,[23,26] indicate the presence of two distinct radical species: rhombic and axial. The rhombic ("type I"[23]) species exhibits three distinct principal components in its EPR **g** tensor ($g_1 = 1.96-1.98$, $g_2 = 2.00$, $g_3 = 2.06-2.08$). On the basis of extensive ENDOR[25]

---

(1) Lippard, S. J.; Berg, J. M. *Principles of Bioinorganic Chemistry*; University Science Books: Mill Valley, CA, 1994.

(2) Chapman, S. K.; Daff, S.; Munro, A. W. *Struct. Bonding* **1997**, *88*, 39.

(3) Borman, S. *Chem. Eng. News* **1999**, *77*, 31.

(4) Hüttermann, J. *EMR of Paramagnetic Molecules*; Berliner, L. J., Reuben, J., Eds.; *Biological Magnetic Resonance 13*; Plenum: New York, 1993; pp 219−252.

(5) Kappl, R.; Hüttermann, J. *Advanced EPR*; Hoff, A. J., Ed.; Elsevier: Amsterdam, 1989; pp 501−540.

(6) Henry, Y.; Lepoivre, M.; Drapier, J.-C.; Ducrocq, C.; Bouchler, J.-L.; Guissani, A. *FASEB J.* **1993**, *7*, 1124.

(7) Marletta, M. A. *Biochemistry* **1994**, *33*, 5636.

(8) Averill, B. A. *Chem. Rev.* **1996**, *96*, 2951.

(9) Upmacis, R. K.; Hajjar, D. P.; Chait, B. T.; Mirza, U. A. *J. Am. Chem. Soc.* **1997**, *119*, 10424.

(10) Kharitonov, V. G.; Sharma, V. S.; Magde, D.; Koesling, D. *Biochemistry* **1997**, *36*, 6814.

(11) Ellison, M. K.; Scheidt, W. R. *J. Am. Chem. Soc.* **1997**, *119*, 7404.

(12) Chan, N.-L.; Rogers, P. H.; Arnone, A. *Biochemistry* **1998**, *37*, 16459.

(13) Ding, X. D.; Weichsel, A.; Andersen, J. F.; Shokhireva, T. Kh.; Balfour, C.; Pierik, A. J.; Averill, B. A.; Montfort, W. R.; Walker, F. A. *J. Am. Chem. Soc.* **1999**, *121*, 128.

(14) Tyryshkin, A. M.; Dikanov, S. A.; Reijerse, E. J.; Burgard, C.; Hüttermann, J. *J. Am. Chem. Soc.* **1999**, *121*, 3396.

(15) Nagatomo, S.; Nagai, M.; Tsuneshige, A.; Yonetani, T.; Kitagawa, T. *Biochemistry* **1999**, *38*, 9659.

(16) Ellison, M. L.; Schulz, C. E.; Scheidt, W. E. *J. Am. Chem. Soc.* **1999**, *38*, 100.

(17) Chen, O.; Groh, S.; Liechty, A.; Ridge, D. P. *J. Am. Chem. Soc.* **1999**, *121*, 11910.

(18) Cheng, L.; Novozhilova, I.; Kim, C.; Kovalevsky, A.; Bagley, K. A.; Coppens, P.; Richter-Addo, G. B. *J. Am. Chem. Soc.* **2000**, *122*, 7142.

(19) Lorkovi, I.; Ford, P. C. *J. Am. Chem. Soc.* **2000**, *122*, 6516.

(20) Scheidt, W. R.; Duval, H. F.; Neal, T. J.; Ellison, M. K. *J. Am. Chem. Soc.* **2000**, *122*, 4651.

(21) Vogel, K. M.; Spiro, T. G. *Biochemistry* **2000**, *39*, 388.

(22) Hayes, R. G.; Eliison, M. K.; Scheidt, W. R. *Inorg. Chem.* **2000**, *39*, 3665.

(23) Morse, R. H.; Chan, S. I. *J. Biol. Chem.* **1980**, *255*, 7876.

(24) Hori, H.; Ikeda-Saito, M.; Yonetani, T. *J. Biol. Chem.* **1981**, *256*, 7849.

10.1021/ic0005691 CCC: $19.00

studies, the rhombic signal has been assigned to a six-coordinated structure, with the nitroso ligand coordinated in a bent end-on orientation and the second axial position filled by an imidazole side chain of a histidine residue. Such an assignment is in agreement with the properties of a model ON−Fe(P)−Im complex,[27] where both EPR and X-ray data are available.[23,28−31] In this complex, the iron atom is displaced from the average porphyrin plane "upward", toward the NO ligand, while the N(NO)−Fe−N(Im) axial direction deviates slightly from the direction perpendicular to the average porphyrin plane.

Despite extensive experimental investigations, the nature of the axial ("type II"[23]) species ($g_{\|} = 1.99-2.00$, $g_{\perp} = 2.02-2.03$) has proven to be more elusive and remains controversial. Several hypotheses of its nature have been advanced, including the following: a complex with an end-on coordinated nitric oxide and approximately C_{4v}-symmetric ON−Fe(P) moiety[4,24] ("linear−bent"); a topological isomer with the Fe atom displaced "below" the porphyrin ligand plane toward the imidazole ligand[23] ("up−down"); a conformation with the N(NO)−Fe−N(Im) axial direction exactly perpendicular to the porphyrin plane[14,26] ("inclined−straight"); an isomer with an elongated Fe−N(Im) axial bond[14] or a completely dissociated five-coordinated nitrosoiron(II) porphyrinate[30] ("bound−dissociated"). Unlike the rhombic species, where the structure of the prototypical model complex is readily available, no simple structurally characterized model has been designed for the axial isomer. Differentiating between the alternative models on the basis of experimental data for biological and noncrystalline systems alone is complicated by strong dynamical effects in type II spectra.[5,32]

At the same time, theoretical techniques are not limited by the synthetic accessibility of model systems and can probe any hypothetical structure directly. Accurate prediction of EPR **g** tensors of small molecules has been possible for some time (see refs 33 and 34 and references therein). However, until recently it was computationally infeasible to provide a nonempirical quantitative connection between a structure of a transition metal complex and its EPR **g** tensor. This restriction has been lifted with the development of density functional (DFT) approaches to the prediction of the EPR **g** tensors.[35,36] DFT techniques were shown to reproduce changes in **g** tensors arising from both major chemical substitutions[37,38] and small variations in ligand environment.[39,40] In favorable cases, the accuracy of calculated changes in **g** components approaches experimental accuracy available from powder EPR spectra.[39]

In this work, we examine the potential energy surfaces (PES) of two model nitrosoiron(II) porphyrins: five-coordinated ON−Fe(P), **1**, and six-coordinated ON−Fe(P)−Im, **2**. The energetic criteria are augmented by calculations of EPR **g** tensors for representative points on the potential energy surfaces, allowing a direct comparison with experimental EPR results. The combined energetic/spectral approach allows us to constrain the values of structural parameters consistent with experimental results to a much narrower range than would be possible with either technique alone. Section 2 of this paper describes computational methods. Sections 3 and 4 examine structures and **g** tensors of complexes **1** and **2**. Section 5 discusses the results and suggests a plausible structural model of the axial species. Finally, section 6 presents the main conclusions of this work.

2. Methods

All calculations are based on DFT[41−43] and were performed with the Amsterdam density functional (ADF) program package,[44−46] using Cartesian space numerical integration[47] and analytical gradients for the geometry optimization.[48,49] The implementation of the EPR **g** tensors is due to Schreckenbach and Ziegler.[35] An uncontracted triple-ζ basis of Slater-type orbitals was employed for the ns, np, nd, $(n + 1)$s, and $(n + 1)$p valence shells of the transition metal elements and the ns, np shells of the main group elements. The basis set was augmented by a set of polarization functions for main group elements and is designated as the standard basis set IV[50] in ADF. Inner shells were treated with the frozen core approximation.[45] Scalar relativistic effects were included in the quasi-relativistic framework[51] employing relativistic frozen core potentials in conjunction with the first-order Pauli Hamiltonian. Molecular geometries were optimized using the VWN[52] local density approximation (LDA) density functional. VWN-optimized geometries of related porphyrin complexes of V, Nb, Cr, and Mo were previously shown to be in a good agreement with experimental results.[39] Relative energies of the structures and bonding energies, which are overestimated by the VWN functional,[42] were obtained through single-point self-consistent calculations employing a gradient-corrected BP86[53,54] functional. EPR **g** tensors were computed using VWN as described elsewhere.[35,55] Calculated **g** tensors of transition metal complexes were previously shown to be essentially independent of the choice of the density functional.[38] All calculations, both in

---

(25) Kappl, R.; Hüttermann, J. *Isr. J. Chem.* **1989**, *29*, 73.

(26) Hüttermann, J.; Burgard, C.; Kappl, R. *J. Chem. Soc., Faraday Trans.* **1994**, *90*, 3077.

(27) Chemical structure abbreviations are the following: Im = imidazole; P = porphyrinato^{2-}; OEP = octaethylporphyrinato^{2-}; TpivPP = pocket fence porphyrin dianion; TPP = tetraphenylporphyrinato^{2-}; Mb = myoglobin; Hb = hemoglobin; PP = protoporphyrin-IX dianion.

(28) Piciulo, P. L.; Rupprecht, G.; Scheidt, W. R. *J. Am. Chem. Soc.* **1974**, *96*, 5293.

(29) Scheidt, W. R.; Frisse, M. E. *J. Am. Chem. Soc.* **1975**, *97*, 17.

(30) Scheidt, W. R.; Piciulo, P. L. *J. Am. Chem. Soc.* **1976**, *98*, 1913.

(31) Nasri, H.; Haller, K. J.; Wang, Y.; Huynh, B. H.; Scheidt, R. *Inorg. Chem.* **1992**, *31*, 3459.

(32) Hagen, W. R. *Advanced EPR*; Hoff, A. J., Ed.; Elsevier: Amsterdam, 1989; pp 785−812.

(33) Bruna, P. J.; Grein, F. *Int. J. Quantum Chem.* **2000**, *76*, 447.

(34) Vahtras, O.; Minaev, B.; Ågren, H. *Chem. Phys. Lett.* **1997**, *281*, 186.

(35) Schreckenbach, G.; Ziegler, T. *J. Phys. Chem. A* **1997**, *101*, 3388.

(36) van Lenthe, E.; Wormer, P. E. S.; van der Avoird, A. *J. Chem. Phys.* **1997**, *107*, 2488.

(37) Schreckenbach, G.; Ziegler, T. *Theor. Chem. Acc.* **1998**, *99*, 71.

(38) Patchkovskii, S.; Ziegler, T. *J. Chem. Phys.* **1999**, *111*, 5730.

(39) Patchkovskii, S.; Ziegler, T. *J. Am. Chem. Soc.* **2000**, *122*, 3506.

(40) van Lenthe, E.; van der Avoird, A.; Hagen, W. R.; Reijerse, E. J. *J. Phys. Chem. A.* **2000**, *104*, 2070.

(41) Parr, R. G.; Yang, W. *Density Functional Theory of Atoms and Molecules*; Oxford University: Oxford, 1989.

(42) Ziegler, T. *Chem. Rev.* **1991**, *91*, 651.

(43) Salahub, D. R.; Castro, M.; Proynov, E. Y. *Relativistic and Electron Correlation Effects in Molecules and Solids*; Malli, G. L., Ed.; Plenum: New York, 1994.

(44) ADF 2.3.3, http://tc.chem.vu.nl/SCM, Department of Theoretical Chemistry, Vrije Universiteit, Amsterdam.

(45) Baerends, E. J.; Ellis, D. E.; Ros, P. *Chem. Phys.* **1973**, *2*, 41.

(46) Fonseca Guerra, C.; Visser, O.; Snijders, J. G.; te Velde, G.; Baerends, E. J. *Methods and Techniques in Computational Chemistry METECC-95* Clementi, E.; Corongiu, G., Eds.; STEF: Cagliari, 1995; pp 305−395.

(47) te Velde, G.; Baerends, E. J. *J. Comput. Chem.* **1992**, *9*, 84.

(48) Versluis, L.; Ziegler, T. *J. Chem. Phys.* **1988**, *88*, 322.

(49) Schreckenbach, G.; Li, J.; Ziegler, T. *Int. J. Quantum Chem. Symp.* **1995**, *56*, 477.

(50) All standard ADF basis sets are available on the Internet at "http://www.scm.com/Doc/atomicdata/".

(51) Ziegler, T.; Tschinke, V.; Baerends, E. J.; Snijders, J. G.; Ravenek, W. *J. Phys. Chem.* **1989**, *93*, 3050.

(52) Vosko, S. H.; Wilk, L.; Nusair, M. *Can. J. Phys.* **1980**, *58*, 1200.

(53) Becke, A. D. *Phys. Rev. A* **1988**, *38*, 3098.

(54) Perdew, J. P. *Phys. Rev. B* **1986**, *33*, 8822; **1986**, *34*, 7406.

geometry optimization and in evaluation of the **g** tensors, employed spin-unrestricted wave functions.

The quasi-relativistic DFT formulation of the EPR **g** tensors used in this work distinguishes among several contributions to the **g** tensor:[35,55]

$$g_{\mathrm{st}} = g_{\mathrm{e}}\delta_{\mathrm{st}} + \Delta g_{\mathrm{st}}^{\mathrm{Rel}} + \Delta g_{\mathrm{st}}^{\mathrm{d}} + \Delta g_{\mathrm{st}}^{\mathrm{p}} \qquad (1)$$

where g_{e} is the free electron g value ($g_{\mathrm{e}} \approx 2.0023$ [56]) and δ_{st} is the Kronecker delta. The term $\Delta g_{\mathrm{st}}^{\mathrm{Rel}}$ combines relativistic corrections arising from the kinetic energy, mass−velocity, and Darwin terms in the quasi-relativistic Hamiltonian.[55,57]

In eq 1, the terms $\Delta g_{\mathrm{st}}^{\mathrm{d}}$ and $\Delta g_{\mathrm{st}}^{\mathrm{p}}$ are, respectively, the diamagnetic and paramagnetic contributions to the **g** tensor. The paramagnetic term $\Delta g_{\mathrm{st}}^{\mathrm{p}}$, which determines deviation of **g** from the free electron value for transition metal complexes, is usually dominated by the magnetic-field-induced coupling between occupied and virtual orbitals and is given by (atomic units)

$$\Delta g_{\mathrm{st}}^{\mathrm{p,occ-vir}} = \frac{g'}{2c}\left\{\int \frac{\partial V_{\mathrm{eff}}(\vec{r})}{\partial(\vec{r})} \times (\vec{j}^{\,s}_{\alpha}(\vec{r}) - \vec{j}^{\,s}_{\beta}(\vec{r}))\,\mathrm{d}\vec{r}\right\}_t \qquad (2)$$

where $g' = 2g_{\mathrm{e}} - 2 \approx 2.0046$, c is the speed of light ($c \approx 137.04$ [57]), V_{eff} is the effective potential experienced by the electrons, and $\vec{j}^{\,s}_{\alpha}$ and $\vec{j}^{\,s}_{\beta}$ are the currents of, respectively, α- and β-spin electrons induced by a unit magnetic field B_s acting in the direction of coordinate axis s ($s = x, y, z$).

The spin−current density for spin γ ($\gamma = \alpha, \beta$) arising from the coupling between occupied and virtual molecular orbitals (MOs) induced by the external magnetic field $\vec{B}_0$ is given by

$$\vec{j}_{\gamma} = \sum_{s=1}^{3} \vec{j}^{\,s}_{\gamma} B_{0,s} = \sum_{s=1}^{3}\sum_{i}^{\mathrm{occ}^{\gamma}}\sum_{a}^{\mathrm{virt}^{\gamma}} u_{ai}^{s,\gamma}\{\Psi_i^{\gamma}\vec{\nabla}\Psi_a^{\gamma} - \Psi_a^{\gamma}\vec{\nabla}\Psi_i^{\gamma}\}B_{0,s} \qquad (3)$$

where Ψ_i and Ψ_a are, respectively, occupied and virtual unperturbed Kohn−Sham orbitals and $u_{ai}^{s,\gamma}$ is the magnetic coupling coefficient between MOs i and a. The principal contribution to $u_{ai}^{s,\gamma}$ is given by[55,58]

$$u_{ai}^{s,\gamma} \approx \frac{1}{2c(\epsilon_a^{\gamma} - \epsilon_i^{\gamma})}\sum_{\nu\lambda} c_{\lambda a}^{\gamma}\, c_{\nu i}^{\lambda}\langle\chi_{\lambda}|[\vec{r}_{\nu} \times \vec{\nabla}]_s|\chi_{\nu}\rangle = \frac{1}{2c(\epsilon_a^{\gamma} - \epsilon_i^{\gamma})}\langle\Psi_a^{\gamma}|\hat{M}_s|\Psi_i^{\gamma}\rangle \qquad (4)$$

where ϵ_a^{γ} and ϵ_i^{γ} are orbital energies of the unperturbed MOs a and i and $c_{\lambda a}^{\gamma}$ and $c_{\nu i}^{\lambda}$ are the unperturbed MO coefficients for the atomic orbitals (AOs) χ_{λ} and χ_{ν}, respectively. Matrix element $\langle\Psi_a^{\gamma}|\hat{M}_s|\Psi_i^{\gamma}\rangle$ represents the first-order magnetic coupling between an occupied molecular orbital i and a virtual orbital a. Within the GIAO formalism, the action of the magnetic coupling operator $\hat{M}_s$ on Ψ_i is simply to apply $i\hat{L}_s^{\nu}$ to each atomic orbital χ_{ν} ($\hat{L}_s^{\nu}$ is the orbital momentum operator centered at ν).

Qualitative analysis of the general eqs 1−4 can be considerably simplified if α and β MOs and corresponding orbital energies are constrained to be identical (spin-restricted approach). In this case, coupling coefficients for α and β MOs become identical according to eq 4. All contributions to $\vec{j}^{\,s}_{\alpha}$ and $\vec{j}^{\,s}_{\beta}$ involving couplings between doubly occupied and fully vacant MOs in eq 2 also become numerically the same so that the corresponding terms for $\Delta g_{\mathrm{st}}^{\mathrm{p,occ-vir}}$ in eq 2 identically cancel. The only surviving spin-restricted contributions to $\Delta g_{\mathrm{st}}^{\mathrm{p,occ-vir}}$ involve coupling between the α component of the singly occupied molecular orbital (α-SOMO,$\Psi_{\mathrm{S}}^{\alpha}$) and virtual α MOs, as well as coupling between occupied β MOs and the (unoccupied) β-SOMO. The expression for $\Delta g_{\mathrm{st}}^{\mathrm{p,occ-vir}}$ is then simplified to

$$\Delta g_{\mathrm{st}}^{\mathrm{p,occ-vir}}\,(\mathrm{restricted}) = \frac{g'}{c}\sum_{a}^{\mathrm{virt}} u_{a,\mathrm{S}}^{s}\left\langle\Psi_{\mathrm{S}}^{\alpha}\left|\left(\frac{\partial V_{\mathrm{eff}}(\vec{r})}{\partial\vec{r}} \times \vec{\nabla}\right)_t\right|\Psi_a\right\rangle - \frac{g'}{c}\sum_{i}^{\mathrm{occ}} u_{\mathrm{S},i}^{s}\left\langle\Psi_i\left|\left(\frac{\partial V_{\mathrm{eff}}(\vec{r})}{\partial\vec{r}} \times \vec{\nabla}\right)_t\right|\Psi_a^{\beta}\right\rangle \qquad (5)$$

The first sum in eq 5 arises from the magnetic-field-induced coupling between the α-SOMO and α virtual MOs and runs over all fully unoccupied MOs. The second sum runs over all doubly occupied MOs and represents the coupling of the fully occupied β MOs with the empty β-SOMO. The operator $\partial V_{\mathrm{eff}}/\partial\vec{r} \times \vec{\nabla}$ appearing in eq 5 is, apart from a constant, the spin-reduced form of the spin−orbit (SO) term in the first-order Pauli Hamiltonian. Matrix elements of this operator are primarily determined by one-center contributions from atomlike regions surrounding the nuclei. The spin−orbit coupling on a nucleus N will then be approximately proportional to the product of the MO coefficients because of AO contributions from the atom N in the MOs connected by the matrix element.

From eqs 4 and 5, to give a sizable contribution to the **g** tensor, an MO must satisfy three conditions: (a) it must have an energy close to the energy of the SOMO so that the denominator in eq 4 is small; (b) the matrix element of the orbital momentum operator $\hat{M}$ (eq 4) between the MO and the SOMO must be large so that the two orbitals can be coupled efficiently by the magnetic field; (c) the spin−orbit matrix element (eq 5) between the orbitals must also be large.

In some of the complexes studied here, the Fe(NO) moiety may undergo a free rotation around the direction perpendicular to the mean porphyrin plane (the Z-axis). In this case, the three principal components of the EPR **g** tensor, which are calculated for a static geometry, have to be averaged according to[39]

$$g_{\|} = \sum_{i=1}^{3} g_i \cos^2 \gamma_z^i \qquad (6)$$

$$g_{\perp} = \frac{1}{2}\sum_{i=1}^{3} g_i \sin^2 \gamma_z^i \qquad (7)$$

where g_i are magnitudes of the principal components of the **g** tensor while γ_z^i is the angle between the direction of the principal component i and Z coordinate axis.

3. Five-Coordinated ON−Fe(P) Structures

We begin by examining the simpler five-coordinated ON−Fe(P) model complex **1**. Because the high-spin $S = {}^3/_2$ state in this system is known to be at least 15 kcal/mol higher in energy than the ground-state spin doublet[59] and is unlikely to influence

---

(55) Schreckenbach, G. Relativity and Magnetic Properties. A Density Functional Study. Ph.D. Thesis, University of Calgary, Calgary, 1996.

(56) Wertz, J. E.; Bolton, J. R. *Electron Spin Resonance*; Chapman and Hall: New York, 1986.

(57) Harriman, J. E. *Theoretical Foundations of Electron Spin Resonance*; Academic Press: New York; 1978.

(58) Schreckenbach, G.; Ziegler, T. *J. Phys. Chem.* **1995**, *99*, 606.

(59) Rovira, C.; Kunc, K.; Hutter, J.; Ballone, P.; Parrinello, M. *J. Phys. Chem. A* **1997**, *101*, 8914.

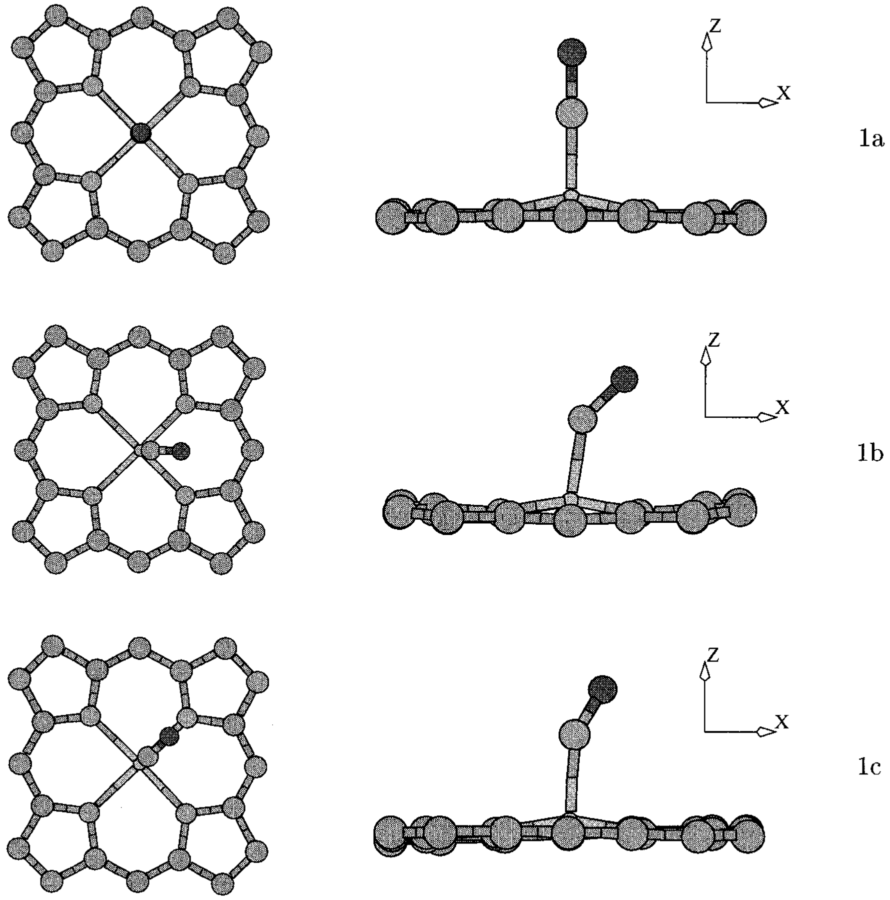

Figure 1. Optimized geometries of five-coordinated nitrosoiron(II) porphyrinate structures **1a**−**1b**. Left view is along the *Z* coordinate axis; right view is along the *Y* coordinate axis. Direction of the *Z* axis coincides with the normal to the average plane of porphyrin nitrogen atoms. The *XZ* plane bisects one of the quadrants of the porphyrin ligand. Positions of hydrogens are not shown for clarity.

Table 1. Selected Structural Parameters[a] and Relative Energies Δ*E* (kcal/mol) for **1a**−**1c**, in Comparison to Experimental Data

	Δ*E*	$R_{\mathrm{Fe-N(NO)}}$	$R_{\mathrm{N=O}}$	$R_{\mathrm{Fe-N_p}}$	Δ(Fe)	Δ(C_m)	$\alpha_{\mathrm{Fe-N}}$	$\alpha_{\mathrm{Fe-N=O}}$	ref
1a	+3.9	1.672	1.163	2.000	0.316	0.026	0.0	180.0	
1b	0.0	1.687	1.172	1.982	0.233	0.155	7.7	142.2	
1c	0.0	1.685	1.171	1.985	0.239	0.015	5.4	144.5	
ON−Fe(OEP)		1.722	1.167	2.004	0.280	0.033	6.2	144.2	11
		1.731	1.168	2.010	0.275	0.040	7.0	142.7	11
ON−Fe(TpivPP)[b]		1.716	1.197	1.981	0.255	0.062	4.9	143	31
			1.258					131	

[a] $R_{\mathrm{Fe-N(NO)}}$ is the iron−nitroso nitrogen bond length (Å); $R_{\mathrm{N=O}}$ is the N=O bond length in the nitroso ligand (Å); $R_{\mathrm{Fe-N_p}}$ is the average equatorial bond length; Δ(Fe) and Δ(C_m) are, respectively, deviation of the position of iron center and the mean absolute deviation of the meso carbon atoms from the mean plane of porphyrin nitrogens (Å); $\alpha_{\mathrm{Fe-N}}$ is the angle between the direction of the Fe−N(O) bond and the Z axis (Figure 1), in degrees; $\alpha_{\mathrm{Fe-N=O}}$ is the Fe−N=O bond angle (in degrees). [b] Partially disordered structure; the first value corresponds to the major conformation.

EPR spectra substantially, only the $S = {}^1/_2$ ground state has to be considered.

3.a. Potential Energy Surface. The coordination of NO around iron gives rise to three key points on the PES of **1**: the C_{4v} structure **1a**, with the linearly coordinated NO ligand; the C_s structure **1b**, with bent end-on coordination of the NO ligand pointing toward one of the meso carbon atoms of the porphyrin ligand; and a second C_s structure **1c**, with the NO bond eclipsing one of the equatorial Fe−N_p bonds. Optimized structures for **1a**−**1c** are illustrated in Figure 1. Their major geometrical features and relative energies are summarized in Table 1, in comparison with the available experimental data.

The porphyrin ligand in the symmetric C_{4v} structure **1a** is essentially planar, with deviation from the mean porphyrin plane not exceeding 0.1 Å. From the normal-mode analysis,[60,61] **1a** is a second-order saddle point rather than a local minimum.[59,62] The doubly degenerate imaginary normal mode corresponds to the symmetry-breaking bending motion of the Fe−N=O fragment, leading to one of the C_s structures **1b** or **1c** or to a range of C_1 structures with an arbitrary orientation of the NO ligand relative to the porphyrin core. Depending on the orientation of the bent NO fragment, the Fe−N=O bond angle in the range 142−145° is obtained upon relaxation of the structure.

Bending of the Fe−N=O bond angle within the symmetry constraints of **1b** is accompanied by an approximately D_{2d} deformation of the porphyrin core, with the two meso carbon atoms located in the symmetry plane moving "up", toward the

---

(60) Wilson, E. B.; Decius, J. C.; Cross, P. C. *Molecular Vibrations*; Dover: New York, 1980.

(61) Fan, L.; Ziegler, T. *J. Phys. Chem.* **1992**, *96*, 6937.

(62) Vogel, K. M.; Kozlowski, P. M.; Zgierski, M. Z.; Spiro, T. G. *J. Am. Chem. Soc.* **1999**, *121*, 9915.

NO ligand by about 0.16 Å, making the porphyrin saddle-shaped. Simultaneously, the direction of the Fe−N(NO) axial bond tilts by about 8° from the Z axis. Structure **1b**, which is similar to the optimized geometries reported for **1** previously,[59,62] is calculated to be approximately 4 kcal/mol more stable than **1a**. From steric considerations, structure **1b** may be expected to be the most energetically favorable. However, in our calculations **1b** is approximately isoenergetic with the eclipsed conformation **1c**, with less than 0.1 kcal/mol energy difference separating the two structures. As a consequence, the NO ligand in free five-coordinated heme nitrosyl **1** should undergo free rotation around the Z axis.

A closer inspection of the optimized structures of **1b** and **1c** reveals that the rotation of the NO ligand is coupled to the distortion of the porphyrin ligand. The maximum deviation from planarity is achieved with NO in the staggered orientation (**1b**), while the eclipsed structure (**1c**) is essentially planar. As a consequence, hindering the D_{2d} distortion of the porphyrin may be expected to increase the barrier for the NO rotation. Indeed, if the porphyrin ligand structure is frozen at the optimized geometry of **1b**, the barrier for NO rotation increases to about 1.2 kcal/mol. The latter value may already be sufficient to freeze the NO rotation on the EPR time scale, at least at low temperatures.

Because a topological isomer of **1** with Fe displaced “below” the porphyrin plane has been proposed as a possible structure of the axial species in this system,[23] we also examined the section of the PES corresponding to the “vertical” motion of the iron center. Although the normal mode corresponding to this distortion is fairly soft, with a force constant of only about 200 kcal mol^{-1} Å^{-2}, it remains harmonic and gives no evidence in favor of a presence of a second minimum along this mode. Similar behavior was previously found for related oxyheme species.[63]

In the presence of several soft modes and given the strong dependence of the internal rotation barrier on the conformation of the porphyrin ligand, the exact orientation of the NO ligand in condensed phases and the position of the iron atom relative to the porphyrin plane are likely to be influenced by intermolecular interactions and substituent effects. Theoretical bond lengths and bond angles are generally in a good agreement with experimental results, although the optimized Fe−N(NO) bond is somewhat too short (calcd, 1.69 Å; exptl,[11,31] 1.72−1.73 Å). In agreement with experimental results,[11] the theoretical structure shows the unusual off-axis tilt of the Fe−N(NO) bond direction. The experimentally observed saddle-shaped distortion of the porphyrin ligand[11,64] is also evident in **1b** but not in the eclipsed **1c**. The large spread in the experimental Fe−N═O bond angles (131−143°) is in accord with the small difference in the calculated energies of the linear and bent structures. In the available high-resolution experimental structures,[11] the NO ligand is preferentially oriented in a position similar to that of **1b**. This preference is likely related to packing constraints rather than to internal conformational preferences of **1**; many five-coordinated nitrosoiron porphyrin structures show a high degree of disorder in the NO orientation.[29,31,64]

3.b. Electronic Structure and g Tensors. The electronic structure of the doublet ground state of **1** is consistent with a d^7 electron count on the iron center[28] (Mulliken d population on iron is 6.7), formally making **1** a complex of Fe(I) with NO$^+$. The unpaired electron occupies a delocalized MO dominated by contributions from d$_{z^2}$ AOs on iron and from π^* orbitals on the NO ligand. Calculated principal components of the **g** tensors are summarized in Table 2, in comparison with available experimental results. The orientations of the **g** tensor components in **1b** and **1c** are given in Table 3, in comparison with the recently reported experimental values.[22]

Table 2. Calculated Principal Components of the **g** Tensors for Five-Coordinated ON−Fe(P) Structures **1a**−**1c**, in Comparison with the Available Experimental Data

		rhombic			axial[a]		
	g_{iso}	g_1	g_2	g_3	$g_\parallel$	$g_\perp$	ref
1a	2.005				2.008	2.003	
1b	2.021	1.994	2.005	2.063	1.998	2.032	
1c	2.018	1.997	2.024	2.033	1.998	2.028	
ON−Fe(TPP)	2.054	2.010	2.064	2.102			69
ON−Fe(TpivPP)	2.06	2.01	2.07	2.11			31
ON−Fe(OEP)	2.059	2.015	2.057	2.106			22

[a] For nonaxially symmetric **1b** and **1c**, axial values are averaged according to eqs 6 and 7.

Table 3. Calculated Direction Cosines[a] for the Principal Components of the **g** Tensors in Five-Coordinated ON−Fe(P) Structures **1b** and **1c**

	g_{ii}	γ_x^i	γ_y^i	γ_z^i
1b	1.994	0.631	0.000	0.776
	2.005	0.776	0.000	−0.631
	2.063	0.000	1.000	0.000
1c	1.997	0.115	0.117	0.987
	2.024	0.691	0.704	−0.163
	2.033	−0.713	0.701	0.000
exptl, 298 K[b]	2.015	−0.159	0.177	0.971
	2.057	0.982	−0.071	0.174
	2.106	0.100	0.981	−0.163

[a] Coordinate system is defined by Figure 1. [b] Data for ON−Fe(OEP) single crystals,[22] transformed into the coordinate system of Figure 1.

As can be seen from Table 2, calculated **g** tensor components are sensitive to the Fe−N═O bond angle. For the linear geometry (**1a**), the **g** tensor deviates very little from the free-electron value. At the same time, structures with the bent Fe−N═O fragment (**1b** and **1c**) show one or two positive principal Δ**g** values. The large difference is somewhat surprising, given that the arrangement of the atoms coordinated directly to the iron remains essentially unchanged. It is instructive to examine the origin of this dependence in terms of individual orbital contributions.

The most qualitatively important contributions to Δ**g** tensors in **1a** and **1b** are compared in Figure 2. In the C_{4v}-symmetric structure **1a**, the singly occupied MO belongs to the totally symmetric a$_1$ representation and is dominated by contributions from iron’s d$_{z^2}$ AOs. This orbital vanishes upon action of the $\hat{M}_z$ operator (eq 4) so that all Δ**g** contributions from **1a** SOMO to the parallel component $\Delta g_\parallel$ also vanish.[65,66] The deviation of the $g_\parallel$ component from the free-electron value is therefore determined by spin-polarization terms. The largest contribution arises from coupling between the b$_1$ nonbonding MO, dominated by the iron’s d$_{z^2-y^2}$ AOs (n$_1$ in Figure 2), and the σ antibonding b$_2$ MO, formed between iron’s d$_{xy}$ AOs and porphyrin (not shown). Calculated energy difference between these MOs is smaller for the β-spin−orbitals (α, 2.63 eV; β, 2.57 eV), resulting in a small positive net contribution to $g_\parallel$.

---

(63) Maréchal, J.-D.; Barea, G.; Maseras, F.; Lledós, A.; Mouawad, L.; Pérahia, D. *J. Comput. Chem.* **2000**, *21*, 282.

(64) Bohle, D. S.; Hung, C.-H. *J. Am. Chem. Soc.* **1995**, *117*, 9584.

(65) Abragam, A.; Bleaney, B. *Electron Paramagnetic Resonance of Transition Ions*; Clarendon: Oxford, 1970.

(66) Mabbs, F. E.; Collison, D. *Electron Paramagnetic Resonance of d Transition Metal Compounds*; Elsevier: Amsterdam, 1992.

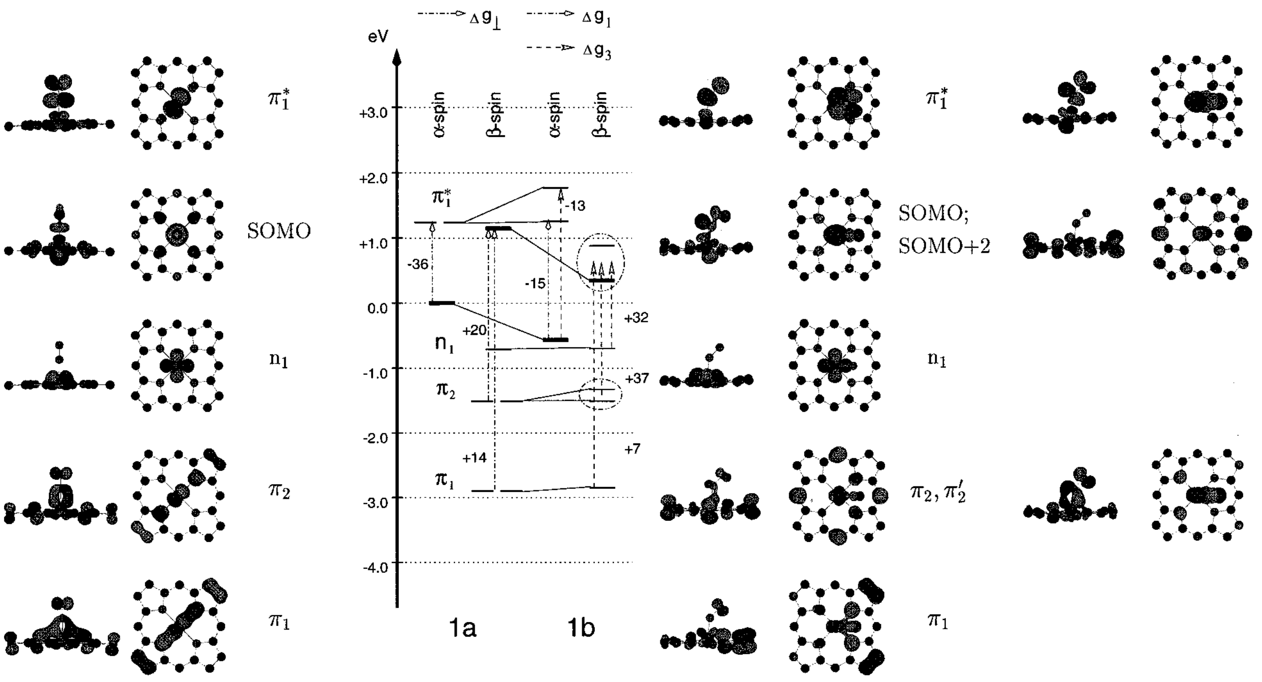

Figure 2. Dominant contributions to the Δ**g** tensor components in **1a** (left) and **1b** (right), in ppt. Kohn−Sham MO energies are given relative to the α-spin part of the SOMO in **1a** (−3.89 eV). On the MO diagram, SOMO is shown in bold. For **1a**, contributions to $\Delta g_{\|}$ involving the d_{z^2}-like SOMO are forbidden by symmetry. The $\Delta g_{\|}$ component in **1a** is dominated by a spin-polarization contribution involving the nonbonding n_1 MO and σ-antibonding MO formed by d_{zy} Fe AOs (not shown); see text. In **1b**, the metal d_{z^2} AOs contribute comparably to two unoccupied β-spin MOs: SOMO and SOMO+2. Both MOs have similar energies and give qualitatively similar contributions to Δ**g**; these contributions are not shown separately. Similarly, contributions arising from two **1b** MOs correlating to the π_2 MOs of **1a** are shown together. The right column of the **1b** MO plots corresponds to higher-energy orbitals. In spin-unrestricted calculations, used presently, the occupued (α-spin) part of the SOMO appears lower in energy than the corresponding unoccupied β-spin orbital. Positions of the MOs that are not qualitatively important for the **g**-tensor results are omitted for clarity.

If the magnetic field in **1a** is oriented in the *XY* plane, the a_1 SOMO can interact with molecular orbitals of e symmetry. The field-induced coupling with π antibonding MOs (d_{xz}, d_{yz}-like) of α-spin, localized on the Fe−N═O fragment, results in a contribution of −36 ppt (parts per thousand) to $g_\perp$. This contribution is almost identically canceled by two β-spin terms (+14 and +20 ppt, respectively) that arise from the coupling between two sets of π-bonding MOs, also showing large contributions from iron d_{xz} and d_{yz} AOs, and the SOMO. Similar magnitudes of the α- and β-spin contributions to $\Delta g_\perp$ in **1a** do not arise from any physical symmetry inherent in this system. Therefore, a perturbation to the electronic structure of **1a**, or a refinement in the theoretical approach,[38] may lead to nonzero $\Delta g_\perp$ contributions.

When the Fe−N═O fragment is bent, forming **1b**, a substantial change occurs in the SOMO composition (Figure 2, right panel). In **1a**, the SOMO exhibits a σ^* character with respect to the Fe−N(NO) and N═O interactions. In the bent **1b**, iron's d_{z^2} AOs show nonzero overlap with the π^* orbitals of the NO ligand. This interaction changes orientation of the d_{z^2}-like contribution to the SOMO toward the direction perpendicular to the NO bond. The resulting angle between the direction of the Fe−N(NO) bond and the d_{z^2}-like component of the SOMO is approximately 20°. The deviation is in the direction *opposite* the direction of the tilt of the Fe−N(NO) bond. Compared to **1a**, the unpaired electron in **1b** is distributed over a larger spatial volume, resulting in stabilization of the SOMO. The degree of spin-polarization is also reduced. The latter is evident in the smaller energy difference between the α SOMO and its β counterpart (**1b**, 0.9 eV; **1a**, 1.1 eV), as well as in the decrease of the Mulliken spin populations on the iron from 1.06 in **1a** to 0.87 in **1b**. Because the energies of other relevant MOs are not strongly affected, stabilization of the SOMO should increase the g_{iso} value of **1b** compared to that of **1a** (see eqs 4 and 5 and Figure 2).

Increased delocalization of the unpaired electron in **1b** decreases the contribution of the iron's d AOs to the SOMO. This produces a substantial d_{z^2}-type contribution to one of the unoccupied β-spin MOs (SOMO+2, 0.5 eV above β-SOMO). In the presence of a magnetic field, this MO interacts with occupied β MOs, giving rise to additional β-spin terms in the **g** tensor. The analogous α-spin MO is not occupied, so no additional α-spin currents arise.

In C_s structure **1b**, three distinct components of the **g** tensor are allowed by symmetry. From ligand field arguments,[66] the orientation of the principal component g_2, showing the smallest deviation from the free-electron value, is expected to coincide approximately with the direction of the d_{z^2}-like contribution to the SOMO. Application of the magnetic field in the *Y* direction, perpendicular to the Fe−N═O plane, can couple a′ SOMO to other a′-symmetric MOs. From comparison with the axial case, a′ components of the π and π^* MOs, correlating with π_1, π_2, and π_1^* MOs in **1a**, may be expected to give substantial contributions. Additionally, tilted orientation of the d_{z^2}-like iron's contribution to the SOMO allows it to couple effectively with occupied nonbonding $d_{z^2-y^2}$ orbital (n_1 in Figure 2). The combination of these factors results in the value of the principal component in the *Y* direction (g_3) being substantially above the free-electron value. The remaining principal component, g_1, is obtained with the magnetic field applied in the direction approximately parallel to the direction of the NO bond.

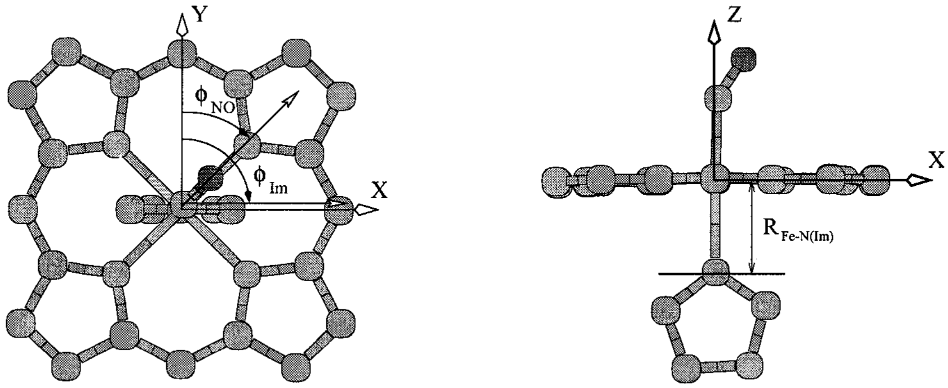

Figure 3. Coordinate system and definition of selected soft structural parameters in the six-coordinated ON−Fe(P)−Im complex **2**. ϕ_{NO} is the angle between projection of the NO bond direction on the average nitrogen plane of the porphyrin ligand and the direction of the *Y* coordinate axis. ϕ_{Im} is the angle between the intersection of the average plane of the imidazole ligand with the *XY* plane and the *Y* coordinate axis. Origin of the coordinate system is on the iron.

This component is dominated by a contribution arising from an α-spin coupling of the unoccupied $a'' \pi^*$ MO, localized on the Fe−N═O fragment, with the SOMO.

Analysis of the MO contributions illustrates the qualitative difference between g_3 and the other principal components in **1b**. The orientation of g_3, which is perpendicular to the Fe−N═O plane, is determined by symmetry. This orientation will remain unchanged if refinements are made to the theoretical procedure or if the system is subjected to a symmetry-conserving perturbation. Orientations of g_1 and g_2, on the other hand, arise from a numerical balance of different contributions of the same symmetry and will change if the magnitudes of the contributions change. Therefore, in the absence of theoretical input, only the orientation of g_3, the largest principal component, can serve as an unambiguous structural indicator in this system.

Contributions of the SOMO $\leftrightarrow$ π and SOMO $\leftrightarrow$ n characters exhibit a qualitatively different dependence on the relative orientation of the NO ligand and the porphyrin core. Shapes of the orbitals with substantial contributions from the metal's d_{xz}, d_{yz}, and d_{z^2} AOs are qualitatively determined by strong interactions within the Fe−N═O fragment. Therefore, such orbitals (SOMO and π-type MOs in Figure 2), as well as their contributions to the **g** tensor, will qualitatively "follow" the orientation of the NO ligand. At the same time, d_{xy} and $d_{x^2-y^2}$ iron AOs decay rapidly outside the *XY* plane and are much less affected by interactions with NO. In **1**, one of these AOs (d_{zy}) participates in σ bonds between iron and the porphyrin ligand, which do not give significant contributions to the **g** tensor in **1**. The remaining orbital ($d_{x^2-y^2}$, n_1 in Figure 2) is nonbonding and is strongly localized on the metal. However, it must maintain orthogonality with the σ-bonding MOs and, therefore, will "follow" the orientation of the porphyrin core rather than the NO ligand. In **1b**, NO is oriented such that both SOMO $\leftrightarrow$ π and SOMO $\leftrightarrow$ n terms contribute to the component of the **g** tensor perpendicular to the FeNO plane. If NO is rotated by 45°, giving **1c**, the SOMO $\leftrightarrow$ π contribution "follows" NO while the SOMO $\leftrightarrow$ n contribution now appears in the direction within the new FeNO plane. As expected from symmetry arguments above, this results in a substantial change in the orientations of g_1 and g_2 components. The g_1 component, which now shows the smallest deviation from the free-electron value, deviates by only 4° from the Fe−N(NO) bond direction (Table 3).

Because of the sensitivity of calculated **g** tensor components to both the Fe−N═O bond angle and the orientation of the NO ligand, it is not particularly surprising that calculated *g* values in **1** are only in a broad qualitative agreement with experimental results (see Table 2). Our calculations succeed in predicting the large positive value and, assuming an orientation of the NO ligand intermediate between **1b** and **1c**, the broad pattern of the *g* values. Nonevertheless, calculated isotropic g_{iso} values are too small compared to experimental results. Part of the deviation may be due to the neglect of the environment effects, which, given the exposed nature of the SOMO, may be substantial in this system.

As may be expected from the substantial discrepancies in the theoretical and experimental magnitudes of the principal components, our calculations are only partially successful in reproducing the experimental orientation[22] of the **g** tensor in this system (see Table 3). The largest component (g_3) is found in the direction perpendicular to the Fe−N═O plane, both in theory and experiment. The experimental angle between the normal to the Fe−N═O plane and the g_3 direction is 9 ± 5°. In agreement with theory, the experimental orientation of the component, closest to the free-electron *g* value, does not coincide with the direction of the Fe−N(NO) bond. However, the magnitude of the deviation is strongly overestimated in our calculations. For **1b**, we calculate an angle of ~20° between g_2 and the Fe−N(NO) bond. The corresponding experimental value is only 8 ± 5°. This discrepancy likely arises from a combination of two factors. First, the calculated angle between the free-electron-like component and the Fe−N(NO) bond direction becomes smaller when NO is displaced from the ideal staggered orientation, decreasing to just 14° for **1c**. In the experimental X-ray structure, NO is displaced slightly from the ideal orientation.[11] Additionally, the calculated magnitudes of g_1 and g_2 in **1b** are almost identical, making their orientation sensitive to small perturbations from the environment.

4. Six-Coordinated NO−Fe(P)−Im Structures

4.a. Potential Energy Surface. Coordination of imidazole in **2** is known to be quite weak.[59,63,67] It is desribed presently by the iron−imidazole distance $R_{Fe-N(Im)}$ and the orientation ϕ_{Im} of the imidazole plane relative to the porphyrin (Figure 3). Potential energy profiles corresponding to a change in the orientation of the NO ligand, with imidazole held in the staggered ($\phi_{Im} = 0°$) or eclipced ($\phi_{Im} = 45°$) conformations are shown in the top panel of Figure 4. In the three distinct local minima (**2a**, $\phi_{Im} = 0°$, $\phi_{NO} = 0°$; **2b**, $\phi_{Im} = 0°$, $\phi_{NO} = \pm 90°$; **2c**, $\phi_{Im} = 0°$, $\phi_{NO} = 180°$), both axial ligands appear in

---

(67) Yoshimura, T.; Ozaki, T.; Shintani, Y.; Watanabe, H. *Arch. Biochem. Biophys.* **1979**, *193*, 301.

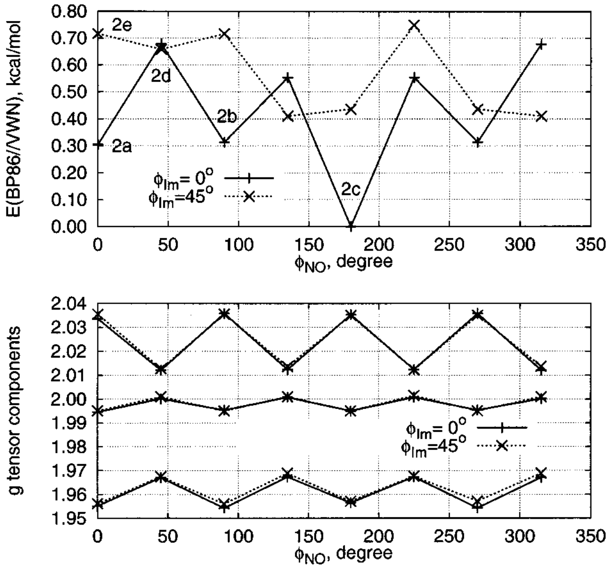

Figure 4. Dependence of the calculated bonding energy (top panel) and principal components of the EPR **g** tensor (lower panel) in **2** on the orientation of axial ligands. Except for ϕ_{NO} and ϕ_{Im}, structures are fully optimized.

staggered orientations. Optimized structures and relative energies of **2a**−**2c**, together with two representative saddle points (**2d**, $\phi_{Im} = 0°$, $\phi_{NO} = 45°$; **2e**, $\phi_{Im} = 45°$, $\phi_{NO} = 0°$), are summarized in Table 4, in comparison with available experimental data.

Conformation **2c**, with both axial ligands located in the *YZ* plane, is the global minimum. However, other staggered/staggered conformations (**2a**, **2b**) appear within 0.3 kcal/mol and will be substantially populated at nonzero temperature. A different preferred relative orientation of the imidazole and NO ligands (**2b**) was obtained in a previous theoretical study.[59] Given the very small energy difference between the local minima, the discrepancy may be safely attributed to the differences in the theoretical procedures. From Figure 4, all relative orientations of axial ligands in gas-phase **2** possess a total energy within 0.8 kcal/mol of the global minimum so that the orientations of NO and imidazole in condensed phases are likely to be determined by substituent effects and intermolecular interactions. In the absence of external constraints, a free rotation of both axial substituents in **2** may also be expected at room or elevated temperatures.

Relative energies of different NO conformations are sensitive to the displacement of the imidazole from its optimal position close to the *Z* axis (Figure 3). If the Fe−N(Im) bond direction is tilted by 20°, while all other structural parameters of the imidazole and porphyrin are fixed at their values in **2b**, the barrier for NO rotation increases by up to 8 kcal/mol. The energetic cost of the distortion is between 20 and 40 kcal/mol, depending on the direction of imidazole tilt.

Dissociation of the imidazole ligand was examined by gradually increasing the iron−imidazole distance, starting from **2b**, and optimizing the remaining structural parameters. The resulting energy profile, given in the top panel of Figure 5, is exceptionally flat. Variations in the Fe−N(Im) bond length between 2.05 and 2.50 Å correspond to total energy changes of less than 1 kcal/mol. As a consequence, experimental bond lengths are likely to be influenced by substitution and environment effects. Although the potential energy profile for the dissociation of imidazole appears to indicate a presence of a local minimum at $R_{Fe-N(Im)} \approx 2.4$ Å, EPR **g** tensors show no qualitative changes in the vicinity of this structure (see below). Therefore, no attempt was made to locate or further characterize this shallow local minimum.

Softness of the imidazole dissociation profile in **2** results in a strong dependence of the theoretical Fe−N(Im) bond length on the computational technique. Thus, VWN density functional using TZP Slater basis set (this work) and B3LYP using a VDZ Gaussian basis set[62] predict $R_{N(Im)} \approx 2.07$ Å. At the same time, geometry optimization using BP86 functional and an augmented plane wave basis set results in a much longer bond length of ∼2.22 Å.[59] Comparable variation in the experimental bond lengths have been observed for similar weakly bound axial ligands (piperidine) in nitrosoiron porphyrins.[68]

With the flatness of the potential energy surface taken into account, the theoretical structure of **2** is in reasonable agreement with the experimental results[28,30] (see Table 4). Experimentally, the imidazole ligand is found to be roughly in the staggered orientation, deviating from the ideal position by about 20°. The minor conformation of the NO ligand ($\phi_{NO} = 2°$) in the experimental structure corresponds directly to **2a**. A similar configuration, with coinciding Fe−N═O and imidazole planes, has been inferred from ENDOR spectra of MbNO.[26] In the major experimental orientation of NO in the model complex ($\phi_{NO} = 124°$), NO is eclipsing one of the Fe−N_p bonds. Other orientations of NO are inaccessible in the experimental structure because of packing constraints.[28,30] The optimized Fe−N(Im) bond length (2.06 Å) is too short compared to the experimental value (2.18 Å[28,30]). However, the calculated increase in total energy upon bond elongation to the experimental value is less than 0.3 kcal/mol, which can be easily accounted for by intermolecular interactions.

The remaining structural parameters are essentially independent of the values of ϕ_{Im} and ϕ_{NO}. Upon addition of the imidazole ligand, the porphyrin ring flattens out, with Δ(Fe) decreasing to 0.06−0.07 Å. This is in good agreement with the experimental value of 0.07 Å. Geometry optimization of an alternative structure, with iron displaced by 0.2 Å "below" the porphyrin plane, converges to the same geometry. The iron atom displacement is strongly dependent on the Fe−N(Im) bond length. At the iron−imidazole separation of 2.85 Å, Δ(Fe) increases to ∼0.20 Å so that the structure of the ON−Fe(P) part of the complex becomes indistinguishable from the free five-coordinated complex **1**. The direction of the Fe−N(NO) bond in **2** almost coincides with the *Z* axis, both in theory and experiment ($\alpha_{Fe-N(NO)}$: calcd, 3.4−4.9°; exptl, 1.8°). Optimized Fe−N(Im) bond direction deviates from the *Z* axis by 0.5−2.0° (exptl, 2°), depending on the local minimum. Calculated Fe−N(NO) bond length increases by ∼0.04 Å (exptl, 0.01−0.02 Å) compared to the five-coordinated complex. The N═O bond length remains essentially unchanged at 1.18 Å (experimental N═O bond lengths in **2** are somewhat uncertain because of the orientational disorder in the structures).

4.b. Calculated g Tensors. Dependence of the calculated EPR **g** tensors on the orientation of imidazole and nitroso ligands in **2** is shown in the bottom panel of Figure 4. For the representative points **2a**−**2e**, the **g**-tensor results are summarized in Table 5. Magnitudes of the **g** tensor principal components vary by less than 3 ppt with changes of ϕ_{Im}, while their orientations change by less than 2°. As a consequence, the orientation of the imidazole ligand will not be discussed from now on.

---

(68) Scheidt, W. R.; Brinegar, A. C.; Ferro, E. B.; Kirner, J. F. *J. Am. Chem. Soc.* **1977**, *99*, 7315.

(69) Wayland, B. B.; Olson, L. W. *J. Am. Chem. Soc.* **1974**, *96*, 6037.

(70) Bruker, E. A.; Olson, J. S.; Ikeda-Saito, M.; Phillips, G. N., Jr. *Proteins: Struct. Funct. Genet.* **1998**, *30*, 352.

Table 4. Selected Structural Parameters[a] and Relative Energies ΔE (kcal/mol) for Representative Points on the Potential Energy Surface of **2**, in Comparison with Experimental Data

	ϕ_{Im}	ϕ_{NO}	ΔE	$R_{\mathrm{Fe-N(NO)}}$	$R_{\mathrm{N=O}}$	$R_{\mathrm{Fe-N_p}}$	Δ(Fe)	Δ(C$_m$)	$\alpha_{\mathrm{Fe-N}}$	$\alpha_{\mathrm{Fe-N=O}}$	$R_{\mathrm{Fe-N(Im)}}$	ref
2a	0	0	+0.3	1.727	1.177	1.988	0.071	0.043	4.9	138.3	2.057	
2b	0	90	+0.3	1.729	1.177	1.987	0.060	0.093	4.6	138.1	2.068	
2c	0	180	0.0	1.727	1.175	1.992	0.070	0.026	4.8	137.7	2.061	
2d	0	45	+0.7	1.726	1.176	1.989	0.071	0.040	3.4	139.9	2.060	
2e	45	0	+0.7	1.726	1.176	1.989	0.079	0.070	4.6	138.3	2.068	
exptl[b]	−18	124		1.742	1.121	2.008	0.071	0.045	1.8	142.2	2.181	28, 30
		2			1.145					138.4		

[a] ϕ_{NO} and ϕ_{Im} define orientations of, respectively, nitroso and imidazole ligands; $R_{\mathrm{Fe-N(Im)}}$ is the iron−imidazole nitrogen bond length (Å); see Figure 3. See Table 1 for definitions of the other structural parameters. [b] ON−Fe(TPP)(**1**−MeIm). First line: major (67%) orientation of the NO ligand. Second line: minor (33%) orientation.

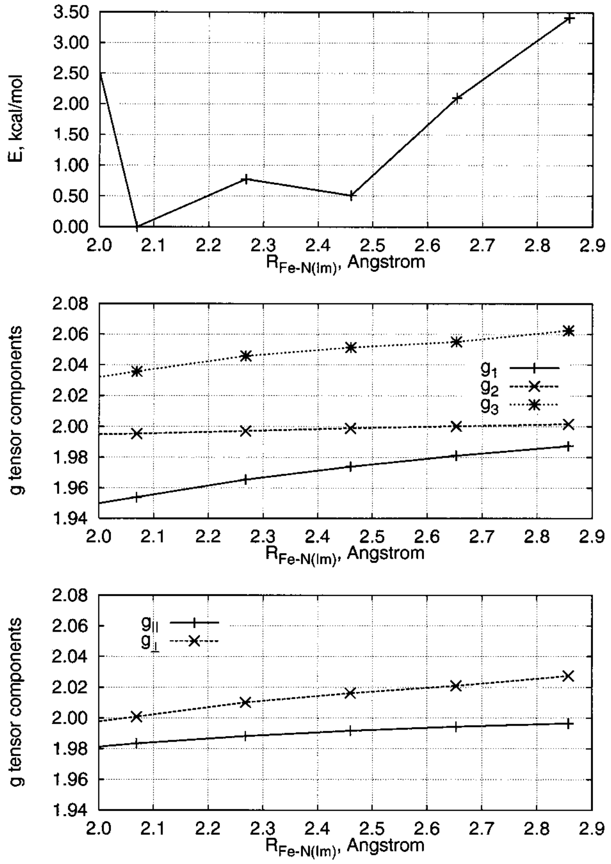

Figure 5. Dependence of the calculated bonding energy (top panel) and **g** tensor components in **2**. Static **g**-tensor components are given on the middle panel. Lower panel shows rotationally averaged parameters (see text). Except for $R_{\mathrm{FeN(Im)}}$, structures are fully optimized. For $R_{\mathrm{FeN(Im)}} > 2.4$ Å, the calculated total energy and **g** tensors are insensitive to the displacements of the imidazole ligand in the *XY* plane.

Table 5. Calculated Principal Components of **g** Tensors for Six-Coordinated ON−Fe(P)−Im Structures **2a**−**2e**, in Comparison with Experimental Data

		rhombic			axial[a]		
	g_{iso}	g_1	g_2	g_3	$g_{\|}$	$g_{\perp}$	ref
2a	1.994	1.955	1.995	2.034	1.983	2.000	
2b	1.995	1.954	1.995	2.036	1.983	2.001	
2c	1.996	1.957	1.995	2.035	1.894	2.001	
2d	1.993	1.967	2.000	2.012	1.983	1.998	
2e	1.996	1.956	1.995	2.036	1.984	2.002	
ON−Fe(PP)−Im	2.015	1.970	2.003	2.072			23
ON−Fe(TPP)−Im	2.018	1.972	2.004	2.079			26
Mb(NO)	2.019	1.979	2.002	2.076			24,25
α-Hb(NO)[b]	2.020	1.974	2.006	2.081			26
β-Hb(NO)[b]	2.014	1.978	2.008	2.057			26

[a] Axial values are obtained according to eqs 6 and 7. [b] α and β chains of nitrosylated hemoglobin.

As in the parent complex **1**, magnitudes of the principal components are sensitive to the orientation of the NO ligand. In the staggered conformation (**2a**−**2c**), principal components are $g_1 \approx 1.96$, $g_2 \approx 2.00$, and $g_3 \approx 2.04$. The largest component (g_3) is in the direction perpendicular to the Fe−N=O plane. The smallest component (g_1) is approximately parallel to the direction of the N=O bond, deviating from it by ~10°. Finally, the component showing the smallest deviation from the free-elector value (g_2) is approximately perpendicular to the NO bond. The direction of g_2 forms an angle of ~40° with the Fe−N(NO) axial bond. In the eclipsed conformation (**2d**), deviations of both the g_1 and the g_3 components from the free-electron value decrease, with $g_1 \approx 1.97$, $g_2 \approx 2.00$, and $g_3 \approx 2.01$. Again, g_3 is found in the direction perpendicular to the Fe−N=O plane. The g_1 component now coincides with the direction of the NO bond to within 2°, and g_2 forms an angle of 40° with the Fe−N(NO) axial bond. If NO is allowed to rotate freely, averaging results in $g_{\|} \approx 1.98$ and $g_{\perp} \approx 2.00$.

For the staggered NO orientation, the dependence of the calculated magnitudes of the principal components on the Fe−N(Im) bond length is given in the middle panel of Figure 5. Elongation of the Fe−N(Im) bond results in an increase in all three principal components. The free-electron-like component (g_2) increases by only 8 ppt/Å in the 2.0−2.9 Å range. The other two components, g_1 and g_3, increase at the rates of, respectively, 45 and 36 ppt/Å. At a separation of 2.9 Å or more, the calculated **g** tensor becomes essentially identical to the result for free five-coordinated species. If the NO ligand rotates freely on the EPR time scale, averaging results in $g_{\perp} > g_{\|}$ (Figure 5, lower panel). The parallel component increases at the rate of 19 ppt/Å. The perpendicular component $g_{\perp}$ grows at 35 ppt/Å so that the separation between the rotationally averaged components increases with dissociation of imidazole.

The qualitative origin of the **g** tensors in **2** is similar to the five-coordinated parent complex (Figure 2). The most significant change arises because of a weak σ^* interaction between a lone pair of the coordinating imidazole nitrogen and the d_{z^2}-like lobe of the SOMO. This interaction results in a relatively small transfer of spin density to imidazole (Mulliken spin population on the coordinating imidazole nitrogen in **2** is ~0.04). Nonetheless, d_{z^2} AOs on iron are destabilized sufficiently to decrease the Mulliken spin population on iron from 0.9 (**1b**) to 0.5 (**2b**). The balance of the spin density shifts to the NO ligand, as illustrated by Figure 6. The energy of the SOMO increases by about 0.9 eV. Other relevant MOs are not noticeably affected by imidazole coordination. The consequences of the change are 3-fold: decrease in the d character of the SOMO reduces the magnitude of the spin−orbit coupling matrix elements, leading to smaller overall deviations from the free-electron g value. At

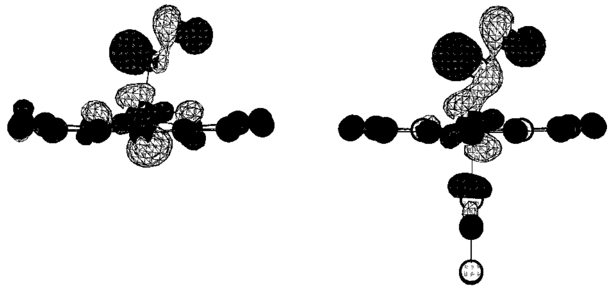

1b
-4.44 eV

2b
-3.53 eV

Figure 6. Change in the SOMO structure upon coordination of imidazole to **1b**.

Table 6. Calculated Direction Cosines[a] for the Principal Components of the **g** Tensors in Representative Six-Coordinated ON−Fe(P)−Im Structures **2**, in Comparison with Experimental Data for "Type I" Heme Nitrosyls

	g_{ii}	γ_x^i	γ_y^i	γ_z^i
2a	1.955	−0.009	0.845	0.534
	1.995	0.001	−0.534	0.845
	2.034	1.000	0.008	0.004
2d	1.967	0.491	0.476	0.730
	2.000	0.534	0.497	−0.684
	2.012	−0.688	0.725	−0.011
Mb(NO), 77K[b]	1.979	0.857	−0.234	−0.459
	2.002	0.430	−0.166	0.888
	2.076	0.283	0.958	0.042

[a] Coordinate system is defined by Figure 3. [b] Data for nitrosyl myoglobin single crystals,[24] direction cosines converted from the crystallographic to the local coordinate system defined by Figure 3 using X-ray structure 1HJT[70] from the Protein Data Bank.

the same time, a large contribution from the NO π^* orbitals to the SOMO of **2** increases the magnitude of matrix elements of the $\hat{M}_s$ operator (eq 4). This accounts for half of the change of the α-SOMO $\leftrightarrow$ $\pi^*_{1,y}$ contribution to g_1 (**1b**, −15 ppt; **2b**, −63 ppt). Finally, the relative destabilization of the SOMO facilitates the magnetic-field-induced mixing of the α-SOMO and α-virtual MOs and decreases the coupling between the β-occupied MOs and the β-SOMO. This, in turn, leads to more negative Δg_1 and Δg_3 values.

For the largest component (Δg_3), electronic contributions due to the imidazole lone pair are partially compensated by an increase in $\pi \leftrightarrow \beta$-SOMO contributions caused by the flattening of the porphyrin in **2**. If imidazole is removed from **2b**, but other structural parameters remain undisturbed, the principal components are calculated to be $g_1 = 2.000$, $g_2 = 2.008$, $g_3 = 2.091$. However, from comparison with **2b** itself ($g_1 = 1.954$, $g_2 = 1.995$, $g_3 = 2.036$) and five-coordinated **1b** ($g_1 = 1.994$, $g_2 = 2.005$, $g_3 = 2.063$), a change in g_1 arises entirely because of electronic interactions.

Theoretical orientations of the **g**-tensor components in **2** are in a good agreement with experimental results for low-temperature "type I" nitroso myoglobin (Table 6). At 77 K, the principal components of the **g** tensor in MbNO[24,25] deviate from the *Z* axis by, respectively, 63 ± 2° (g_1), 27 ± 2° (g_2), and 88 ± 2° (g_3). The corresponding theoretical values for free **2a** are 58°, 32°, and 90°. Comparison of the remaining experimental γ_a^i values with the theoretical results gives ϕ_{NO} of approximately −70° in MbNO. Calculated magnitudes of the **g** principal components in **2** appear to be in a broad qualitative agreement with experimental results. The characteristic $g_1 < \mathrm{g}_2\ (\sim g_e) \ll g_{\max}$ pattern is reasonably well reproduced. At the same time, calculated values are too small compared to experimental results, by 20−50 ppt.

5. Discussion: Structural Models of the Rhombic and Axial Species

Examination of the EPR **g** tensors and potential energy surfaces of five- and six-coordinated nitrosoiron porphyrin complexes suggests the following structural interpretation of the experimental EPR parameters for biological heme nitrosyl adducts.

Rhombic Signal. The rhombic signal ("state I") exhibits a characteristic pattern of $g_{\min} < g_{\mathrm{free}} \ll g_{\max}$.[5,14,23−26] This pattern appears to correspond to the six-coordinated complex **2** with the internal rotation of the NO ligand frozen on the EPR time scale. Calculated orientations of the principal components for the staggered conformation of the complex **2a** are in an excellent agreement with the experimental result for nitrosylated myoglobin (MbNO) single crystals. At low temperatures, the direction of the g_2 component in MbNO deviates by ∼30° from the average normal to the porphyrin plane.[24,25] The value calculated at the theoretical *gas-phase* geometry of the model complex **2** is 32°, suggesting that the ON−Fe(P) fragment in MbNO is not noticeably distorted by interactions with the protein environment. The large inclination of the g_2 component has been previously attributed[4,5,14,24−26] to a large-angle distortion of the Fe−N(NO) bond direction in biological heme nitrosyls. Despite a good agreement between the theoretical and experimental **g** orientations, calculated magnitudes of the principal components ($g_1 = 1.95$, $g_2 = 2.00$, $g_3 = 2.04$) are only in a qualitative agreement with the experimental results (MbNO at 77 K:[24,25] $g_1 = 1.98$, $g_2 = 2.00$, $g_3 = 2.08$). The errors in the g_1 and g_2 components may be partially attributed to the too short theoretical iron−imidazole bond length in **2** (calcd, 2.06 Å; exptl, 2.18 Å). The larger error in the g_3 component likely indicates strong environmental effects such as coordination of NO by a proximal histidine residue.[14] Sensitivity of the g_1 and g_3 components to environmental influences is experimentally well documented for type I heme nitrosyl systems. Measured g_1 values for such systems range from 1.97 (ON−Fe(TPP)−Im in DMF[23]) to 1.99 (MbNO[26]). Comparable dependence is found for g_3, from 2.06 (α-chain of HbNO[26]) to 2.08 (β-chain of HbNO[26]).

Axial Signal. The axial signal ("state II") exhibits smaller experimental variability in the EPR **g** tensor components. It is observed[14,23,26] as a sharp signal at $g_{\parallel} \approx 1.99$, together with a broader component at $g_{\perp} \approx 2.02-2.04$. These features are, in principle, consistent with two structural models. The only acceptable static interpretation involves a structure with the NO ligand eclipsing one of the equatorial Fe−N$_\mathrm{p}$ bonds. Depending on the Fe−N(Im) bond length, calculated principal components range from $g_{\parallel} = 1.97$, $g_{\perp} = 2.00$, and $g'_{\perp} = 2.01$ (imidazole bound, **2d**) to $g_{\parallel} = 2.00$, $g_{\perp} = 2.02$, and $g'_{\perp} = 2.03$ (imidazole dissociated, **1c**). A static interpretation may be tenable for some of the biological nitrosoheme systems, where the protein environment of the prosthetic group may, at least in principle, sterically constrain the NO moiety to the eclipsed orientation. However, this model fails to provide a realistic explanation for the appearance of the type II spectra in model ON−Fe(P)−Im complexes at higher temperatures.[23] These complexes lack the versatile protein environment and therefore cannot be reasonably expected to switch from favoring the staggered conformation at low temperatures to preferring the eclipsed NO orientation at near-room temperatures. Moreover, calculated separations between the $g_{\perp}$ and $g'_{\perp}$ components in eclipsed structures are sufficiently large to allow these components to be individually discernible in experimental spectra, which does not appear to be the case.

Other proposed static interpretations of type II spectra appear to be inconsistent with the theoretical results. The “up−down”,[23] “linear−bent”,[4,24] and “inclined−straight”[14,26] models postulate the existence of stable local minima not present on the theoretical potential energy surface. For the first two models, the theoretical potential energy surface is sufficiently steep to make appearance of the required local minima upon chemical substitution unlikely. In the presence of additional chemical bonds tethering imidazole to the protein backbone, the local minima postulated in the “inclined−straight” model may be realizable in biological systems. However, rhombic, rather than axial, values of the components of **g** are then computed for the suggested structure of the type II species. The “up−down” and “bound−dissociated”[14,30] models of type II species are also predicted to exhibit rhombic **g** tensors.

Type II spectra are usually encountered at higher temperatures, where large displacements along various low-energy normal modes of **1** and **2** may become significant. Therefore, it appears reasonable to consider possible *dynamical* interpretations. The intramolecular rotation of the NO ligand around the Z axis is associated with particularly small activation barriers, both in **1** and in **2**. If the rotation is unfreezed on the EPR time scale, averaging of the **g** components leads to an axial spectrum (see above). Depending on the iron−imidazole bond length, calculated magnitudes of the principal components range from $g_{\|} \approx 1.98$, $g_{\perp} \approx 2.00$ (imidazole bound, **2**) to $g_{\|} \approx 2.00$, $g_{\perp} \approx 2.03$ (imidazole dissociated, **1**), as illustrated in the lower panel in Figure 5. If the bond is only partly dissociated, with $R_{\mathrm{Fe-N(Im)}} \approx 2.5$ Å, rotationally averaged magnitudes of the principal components appear to be in a good qualitative agreement with experimental results. From the calculated potential energy surface, such bond elongation requires less than 1 kcal/mol, compared to the equilibrium structure.

In the model ON−Fe(P)−Im complex, the imidazole ligand has no additional chemical bonds to the ON−Fe(P) fragment and will dissociate completely. In this case, type II spectra in the model system would arise from the five-coordinate species in a local environment facilitating rotational motion of the NO ligand. In heme-containing proteins, on the other hand, imidazole is provided by a histidine residue and is tethered to the backbone. The tethering may prevent a complete dissociation of the imidazole, which would therefore result in smaller values of $g_{\|}$ and $g_{\perp}$, compared to the fully dissociated system. Variations in the magnitudes of **g** tensor components between different proteins would also be expected. Indeed, experimental type II values of the components of **g** in nitrosoheme proteins tend to be lower than in the model system (α-HbNO, $g_{\perp} = 2.024$;[26] β-HbNO, $g_{\perp} = 2.033$;[26] ON−Fe(P)−Im, $g_{\perp} = 2.043$ [23]). In this model, tethering of the imidazole to the backbone would allow the protein to switch between type I and type II spectra at the same temperature. A conformational change in the backbone can pull the imidazole from the rest of the complex, effectively causing its dissociation. This would, in turn, lower the barrier for NO rotation and produce the change in the spectrum. Type I to type II spectral changes are well documented in hemoglobin[26] upon the R/T transformation. From ENDOR results, the transformation is believed to be accompanied by an increase in the iron−imidazole bond length.[26]

6. Conclusions

In both five- and six-coordinated complexes, the NO ligand is preferably coordinated end-on, with a Fe−N═O bond angle of approximately 140°. The flipping motion of the NO ligand is associated with an activation barrier of ∼4 kcal/mol. In the *gas-phase* five-coordinated complex, NO is predicted to undergo free rotation. Coordination with imidazole in the second axial position increases the gas-phase barrier for NO rotation to about 1 kcal/mol. The barrier is further increased if imidazole is displaced within the XY plane from its equilibrium position close to the Fe−N(NO) bond direction. Elongation of the iron−imidazole bond from 2.07 Å (optimized structure) to 2.5 Å increases total energy by less than 1 kcal/mol. Experimental orientations of both axial ligands, and the Fe−N(Im) bond length, are likely to be strongly influenced by intermolecular interactions and packing effects.

In contrast to the total energy, calculated EPR **g**-tensors are sensitive to the orientation of the NO ligand and Fe−N(Im) bond length. With NO in the staggered orientation, calculated **g** tensor components range from $g_1 = 1.994$, $g_2 = 2.005$, $g_3 = 2.063$ (five-coordinated, **1**) to $g_1 = 1.955$, $g_2 = 1.995$, $g_3 = 2.035$ (six-coordinated, **2**). In the eclipsed conformation, **g** tensor components vary from $g_1 = 1.997$, $g_2 = 2.024$, $g_3 = 2.033$ (in **1**) to $g_1 = 1.967$, $g_2 = 2.000$, $g_3 = 2.012$ (in **2**). Calculated **g** tensors are not sensitive to the orientation of the imidazole ligand.

Orientation of the **g**-tensor component, showing the smallest deviation from the free-electron value, does not coincide with the direction of the axial Fe−N(NO) bond. For the staggered five-coordinated structure (**1b**), the two directions differ by ∼20°. The deviation increases to almost 40° for the six-coordinated species (**2a**). Calculated orientations of the principal components of the **g** tensor in the six-coordinated species are in good agreement with experimental results for nitrosomyoglobin.[24] At the same time, calculated magnitudes of the individual principal components are too low, by up to 50 ppt, compared to experimental results. Errors in the calculated **g** tensors likely arise from environmental influences.

From comparison of the calculated and experimental **g** tensors, the rhombic (“type I”) EPR signal in nitrosoheme systems can be assigned to a static structure with NO oriented toward the meso-C atom of the porphyrin ring and $R_{\mathrm{Fe-N(Im)}} \approx 2.1$ Å (calcd, $g_1 = 1.95$, $g_2 = 2.00$, $g_3 = 2.04$; exptl, $g_1 = 1.96-1.98$, $g_2 = 2.00$, $g_3 = 2.06-2.08$). The ON−Fe(P) moiety in biological type I species does not appear to be noticeably distorted by the protein environment. The axial (“type II”) EPR signal is tentatively assigned to a partially dissociated species ($R_{\mathrm{Fe-N(Im)}} \approx 2.5$ Å), with a freely rotating NO ligand (calcd, $g_{\|} = 2.00$, $g_{\perp} = 2.03$; exptl, $g_{\|} = 1.99-2.00$, $g_{\perp} = 2.02-2.03$).

The structural and electronic flexibility of the nitrosoheme moiety makes a full-system simulation, including steric and electrostatic effects due to the protein environment, neceessary for the accurate theoretical prediction of EPR properties in this system. It might provide an exciting, and challenging, the target for a future simulation.

Acknowledgment. This work has been supported by the National Sciences and Engineering Research Council of Canada (NSERC), as well as by the donors of the Petroleum Research Fund, administered by the American Chemical Society (ACS PRF 31205-AC3).

Supporting Information Available: Optimized Cartesian structures of **1a**−**1c** and **2a**−**2e**. This material is available free of charge via the Internet at http://pubs.acs.org.

IC0005691